Response of the Amazon carbon balance to the 2010 drought derived with CarbonTracker South America

I.T. van Der Laan-Luijkx, I.R. van Der Velde, M.C. Krol, L.V. Gatti, L.G. Domingues, C.S.C. Correia, J.B. Miller, M. Gloor, T.T. van Leeuwen, J.W. Kaiser, et al.

AGU PUBLICATIONS

Global Biogeochemical Cycles

RESEARCH ARTICLE
10.1002/2014GB005082

Special Section:
Trends and Determinants of the Amazon Rainforests in a Changing World, A Carbon Cycle Perspective

Response of the Amazon carbon balance to the 2010 drought derived with CarbonTracker South America

I. T. van der Laan-Luijkx[1], I. R. van der Velde[1], M. C. Krol[1,2,3], L. V. Gatti[4], L. G. Domingues[4], C. S. C. Correia[4], J. B. Miller[5,6], M. Gloor[7], T. T. van Leeuwen[2,3,8], J. W. Kaiser[9], C. Wiedinmyer[10], S. Basu[5,6], C. Clerbaux[11], and W. Peters[1,12]

[1]Meteorology and Air Quality, Wageningen University, Wageningen, Netherlands, [2]Institute for Marine and Atmospheric Research Utrecht, Utrecht University, Utrecht, Netherlands, [3]SRON Netherlands Institute for Space Research, Utrecht, Netherlands, [4]Instituto de Pesquisas Energéticas e Nucleares (IPEN), Centro de Química Ambiental, São Paulo, Brazil, [5]Global Monitoring Division, Earth System Research Laboratory, National Oceanic and Atmospheric Administration (NOAA), Boulder, Colorado, USA, [6]Cooperative Institute for Research in Environmental Sciences (CIRES), University of Colorado, Boulder, Colorado, USA, [7]School of Geography, University of Leeds, Leeds, UK, [8]Faculty of Earth and Life Sciences, VU University Amsterdam, Amsterdam, Netherlands, [9]Max Planck Institute for Chemistry, Mainz, Germany, [10]National Center for Atmospheric Research (NCAR), Boulder, Colorado, USA, [11]LATMOS-IPSL, UPMC University Paris 06, Université de Versailles Saint-Quentin-en-Yvelines, CNRS/INSU, Paris, France, [12]Centre for Isotope Research, University of Groningen, Groningen, Netherlands

Key Points:
- Amazon carbon budget estimated by CarbonTracker South America
- Biospheric uptake decreases by 0.08–0.26 PgC/yr in response to 2010 drought
- Amazon biomass burning emissions more than doubled during 2010 drought

Supporting Information:
- Figures S1–S7, Text S1, and Table S1

Correspondence to:
I. T. van der Laan-Luijkx,
ingrid.vanderlaan@wur.nl

Citation:
van der Laan-Luijkx, I. T., et al. (2015), Response of the Amazon carbon balance to the 2010 drought derived with CarbonTracker South America, *Global Biogeochem. Cycles*, *29*, 1092–1108, doi:10.1002/2014GB005082.

Received 30 DEC 2014
Accepted 1 JUL 2015
Accepted article online 2 JUL 2015
Published online 30 JUL 2015

Abstract Two major droughts in the past decade had large impacts on carbon exchange in the Amazon. Recent analysis of vertical profile measurements of atmospheric CO_2 and CO by Gatti et al. (2014) suggests that the 2010 drought turned the normally close-to-neutral annual Amazon carbon balance into a substantial source of nearly 0.5 PgC/yr, revealing a strong drought response. In this study, we revisit this hypothesis and interpret not only the same CO_2/CO vertical profile measurements but also additional constraints on carbon exchange such as satellite observations of CO, burned area, and fire hot spots. The results from our CarbonTracker South America data assimilation system suggest that carbon uptake by vegetation was indeed reduced in 2010 but that the magnitude of the decrease strongly depends on the estimated 2010 and 2011 biomass burning emissions. We have used fire products based on burned area (Global Fire Emissions Database version 4), satellite-observed CO columns (Infrared Atmospheric Sounding Interferometer), fire radiative power (Global Fire Assimilation System version 1), and fire hot spots (Fire Inventory from NCAR version 1), and found an increase in biomass burning emissions in 2010 compared to 2011 of 0.16 to 0.24 PgC/yr. We derived a decrease of biospheric uptake ranging from 0.08 to 0.26 PgC/yr, with the range determined from a set of alternative inversions using different biomass burning estimates. Our numerical analysis of the 2010 Amazon drought results in a total reduction of carbon uptake of 0.24 to 0.50 PgC/yr and turns the balance from carbon sink to source. Our findings support the suggestion that the hydrological cycle will be an important driver of future changes in Amazonian carbon exchange.

1. Introduction

The carbon balance of Amazonia plays an important role in the budget of the atmospheric greenhouse gases CO_2 and CH_4. This is because the Amazon holds a vast amount of aboveground biomass [e.g., *Malhi et al.*, 2006; *Gloor et al.*, 2012], contains the largest area of wetlands worldwide [e.g., *Richey et al.*, 2002], and has a much larger annual carbon uptake and release than is typical for extratropical ecosystems [e.g., *Araujo et al.*, 2002; *Pan et al.*, 2011]. Changes in precipitation, radiation, and temperature significantly affect the terrestrial carbon cycle in Amazonia and are known drivers of short-term changes in global growth rates of CO_2 [e.g., *Conway et al.*, 1994; *Wang et al.*, 2013] and CH_4 [*Nisbet et al.*, 2014]. This is for instance due to the El Niño Southern Oscillation, which can bring droughts to parts of the region leading to increased tree mortality [*Phillips et al.*, 2009] and biomass burning [*van der Werf et al.*, 2008]. Interactions between droughts and the carbon cycle is a key uncertainty in current climate models [*Booth et al.*, 2012; *Cox et al.*, 2013; *Piao et al.*, 2013] that could strongly influence the rate of atmospheric CO_2 increase over the next decades [*Ciais et al.*, 2013].

Consequently, many efforts are ongoing to better understand the Amazonian carbon balance. These range in scale from fairly local, such as eddy-covariance measurements of energy, water, and carbon

fluxes [e.g., *Araujo et al.*, 2002; *Saleska et al.*, 2003; *Kruijt et al.*, 2004], to larger scales, such as the Brazilian land use change monitoring program and the repeated survey of hundreds of forest plots across South America through RAINFOR [*Malhi et al.*, 2002]. An overview of such efforts and their results is given in *Gloor et al.* [2012]. Increasingly, remote sensing observations such as burned area, fire hot spots, aboveground standing biomass, canopy greenness, and fluorescence are used to study the Amazon forest [*Saatchi et al.*, 2008, 2013; *Lee et al.*, 2013; *Parazoo et al.*, 2013]. Integration of such diverse measurements over the wide range of scales is often complicated by the large heterogeneity in almost any soil or vegetation trait across Amazonia. As a result, carbon cycle modeling of this region is challenging, and uncertainty on its current and future interactions with climate is large.

Amazonia experienced two recent severe drought events, the first in 2005 and the second in 2010 [*Lewis et al.*, 2011; *Potter et al.*, 2011; *Xu et al.*, 2011]. During both events the ground-based RAINFOR forest surveys provided an estimate of the drought impact on tree growth and mortality. They showed that severe droughts cause a strong deviation from the long-term positive biomass increments measured in the two preceding decades. Reduced growth and increased tree mortality were observed across the network even in years after the drought event [*Phillips et al.*, 2009, 2010]. This resulted in additional carbon loss, partly to the atmosphere, of 1.0 to 1.6 PgC from each event, with a sizable fraction estimated to occur in the drought year itself.

Independent estimates of the carbon balance in a part of the Amazon for the period 2000–2009 were presented by *Gatti et al.* [2010] based on vertical profile measurements of the mole fractions of CO_2 and CO from Santarém, Brazil. The rapid vertical mixing of CO_2 surface exchange signals allowed a climatological net terrestrial carbon balance to be inferred, suggesting that a biomass burning CO_2 source from the area is countered by net uptake in the terrestrial biosphere, in broad agreement with independent results [*Saleska et al.*, 2003; *Pyle et al.*, 2008]. Since then, more years of data have been collected from this Santarém aircraft program, and more importantly, it was expanded to include three additional sampling sites. The first full year that this network was in place was during the 2010 drought, and it has been continued since then, resulting in a recent publication by *Gatti et al.* [2014]. They provide a quantitative estimate of the response of terrestrial vegetation in the Amazon to the 2010 drought.

The *Gatti et al.* [2014] estimate was observation based and uses the observations of CO_2 and CO (as well as SF_6) to calculate fluxes. Fire emissions were estimated using the observed CO:CO_2 ratios. This approach suggested a total drought impact on the Amazon net carbon exchange of nearly 0.50 PgC in 2010 compared to 2011, with an increase in carbon release due to biomass burning (+0.25 PgC/yr) and a reduction of carbon uptake by vegetation (0.22 PgC/yr). The latter suggests a strong drought response of tropical vegetation.

In this study, we revisit these findings and interpret not only the same CO_2/CO vertical profile measurements but also additional constraints on carbon exchange from satellite observations of CO, burned area, fire hot spots, photosynthetically active radiation (PAR), and leaf area index. An important tool in this interpretation is the CarbonTracker data assimilation framework for South America specifically developed for this application. It quantitatively links detailed surface CO_2 exchange simulations to the observed profiles, through the TM5 atmospheric transport model at $1° \times 1°$ horizontal resolution. This effort presents the first attempt to fully integrate the CO_2 and CO observations from the Amazon with our spatiotemporal knowledge of fires and biospheric CO_2 exchange in the region.

Following our description of the newly developed CarbonTracker South America system (section 2), we proceed to describe its results in comparison to independent fire emission estimates (section 3.1) as well as to atmospheric mole fraction observations of CO and CO_2 in and around South America (sections 3.2 and 3.3). The final Amazon carbon balance estimates produced from a number of different system configurations are presented next (section 3.4), followed by a discussion of our results (section 4) and conclusions (section 5).

2. Methods

2.1. CarbonTracker South America

To study the Amazon carbon cycle using inverse modeling, we have adapted the CarbonTracker data assimilation system [*Peters et al.*, 2007] to create the dedicated version "CarbonTracker South

America" (CT-SAM). CT-SAM uses the atmospheric transport model TM5 [*Peters et al.*, 2004; *Krol et al.*, 2005] to transport a set of prior carbon fluxes globally, and the obtained atmospheric CO_2 mole fractions are compared to a large set of atmospheric observations. The differences between the simulated and observed mole fractions are subsequently minimized by changing the fluxes using an ensemble Kalman filter data assimilation technique. CT-SAM optimizes the set of prior CO_2 fluxes according to

$$F(x,y,t) = \lambda_r \cdot F_{bio}(x,y,t) + \lambda_r \cdot F_{oce}(x,y,t) + F_{ff}(x,y,t) + F_{fire}(x,y,t) \quad (1)$$

where F_{bio}, F_{oce}, F_{ff}, and F_{fire} are the prior terrestrial biosphere, ocean, fossil fuel, and biomass burning carbon fluxes, respectively, and λ_r are weekly linear scaling factors that are optimized in the assimilation for each region (see section 2.5). CarbonTracker only solves for the biosphere and ocean fluxes, whereas the fossil fuel and biomass burning fluxes are imposed and assumed to be known. Because biomass burning dominates the carbon balance in South America, we have performed simulations with four alternative sets of imposed biomass burning fluxes, one of which was optimized using (satellite) observations of CO mole fractions in a separate inverse modeling framework. More details are described in section 2.6.

We have performed a set of atmospheric inversions focusing on the 2010–2011 period using different setups of CT-SAM, which are described in more detail in section 2.7. In the following sections we will focus on the specific characteristics of CT-SAM. For more general details on the CarbonTracker system, see *Peters et al.* [2007] and http://www.carbontracker.eu.

2.2. Prior Flux Estimates

The prior biosphere carbon fluxes [net biome exchange (NBE), i.e., the nonfire terrestrial vegetation fluxes] that we use as input in CT-SAM are from the SiBCASA model [*Schaefer et al.*, 2008; *van der Velde et al.*, 2014]. The SiBCASA model is a combination of the Simple Biosphere model (SiB), version 3 [*Sellers et al.*, 1996] and the Carnegie-Ames-Stanford Approach (CASA) model [*Potter et al.*, 1993]. The SiB model provides the biophysical part, and the biogeochemistry is from the CASA model. These two combine into the SiBCASA model, which simulates the carbon fluxes of the terrestrial biosphere on a horizontal resolution of $1^\circ \times 1^\circ$ with a 10 min time step. Important inputs for the SiBCASA model are the meteorological drivers of carbon exchange and the satellite-observed normalized difference vegetation index. In CT-SAM we use the resulting NBE fluxes on a three hourly time step as input and optimize them at a weekly time resolution.

In this study we use four different sets of biomass burning emissions. The first is also modeled by SiBCASA [*van der Velde et al.*, 2014], following the work of *van der Werf et al.* [2010]. Daily burned area estimates from the Global Fire Emissions Database version 4 (GFED4) [*Giglio et al.*, 2013] are used in combination with maps of vegetation types, the modeled carbon stocks from SiBCASA, and an estimate of the combustion completeness. The GFED4 burned area estimates are based on the observations of fire counts by the Moderate Resolution Imaging Spectroradiometer (MODIS) instrument. The full data set was produced by combining 500 m MODIS burned area maps with active fire data from the Tropical Rainfall Measuring Mission, the Visible and Infrared Scanner, and the Along-Track Scanning Radiometer. The second and third sets of biomass burning emissions are from the Global Fire Assimilation System (GFAS) version 1 [*Kaiser et al.*, 2012], which are based on fire radiative power, and those from the Fire Inventory from NCAR (FINN) version 1 [*Wiedinmyer et al.*, 2011] based on fire hot spots. For details we refer to the provided references. The fourth set are the results of the optimization of the SiBCASA-GFED4 emissions using (satellite) CO observations (section 2.6).

The contribution of fossil fuels to the carbon budget of South America is very small compared to the biosphere fluxes and biomass burning emissions. The fossil fuel fluxes used in CT-SAM are emissions from the *EDGAR4.2* database [2011], together with country- and sector-specific time profiles derived by the Institute for Energy Economics and the Rational Use of Energy from the University of Stuttgart and constructed for the CARBONES project (http://www.carbones.eu/).

The prior ocean carbon fluxes are calculated from the monthly air-sea differences in partial pressure of CO_2 obtained from the ocean inversions described by *Jacobson et al.* [2007], combined with a three hourly time step of the gas transfer velocity computed from wind speeds in the atmospheric transport model. The resulting ocean carbon fluxes are optimized for 30 different ocean inversion regions.

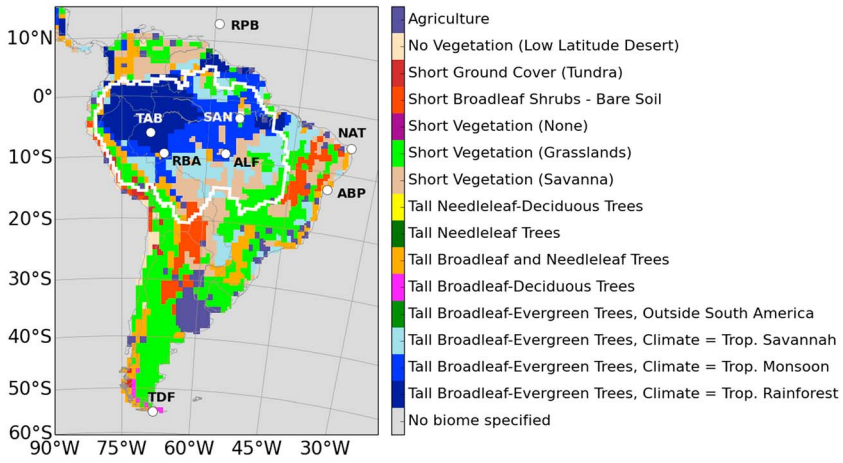

Figure 1. Map of the land cover used in the SiBCASA model. For the calculation of the prior covariance structure in CT-SAM, the Tall Broadleaf-Evergreen Trees biome within South America was further split up in three different climate zones according to the Köppen climate classification system [*Kottek et al.*, 2006]. The white contour shows the selection of the Amazon region.

2.3. Atmospheric Transport

The atmospheric transport model TM5 [*Krol et al.*, 2005] was set up with a global horizontal resolution of 6°×4° (longitude by latitude) and nested zoom grids of 3°×2° and 1°×1° over South America (see supporting information for details). The meteorological driver data are from the ERA-interim re-analysis [*Dee et al.*, 2011] on a three hourly time resolution and 25 vertical levels, obtained from the European Centre for Medium-Range Weather Forecasting (ECMWF). In contrast to earlier versions of TM5, the convective entrainment and detrainment fluxes are obtained directly from the ERA-interim data from ECMWF, which was found to improve the inter-hemispheric exchange of tracers in the TM5 model.

2.4. Observations

To optimize the prior CO_2 fluxes, we use a large set of atmospheric CO_2 observations from a global network of monitoring stations. For CT-SAM the most important observations are those from the unique flask sampling program in the Amazon run by the Instituto de Pesquisas Energéticas e Nucleares (IPEN), São Paulo, Brazil, in collaboration with the National Oceanic and Atmospheric Administration (NOAA) Global Monitoring Division, Boulder, Colorado, USA. Vertical profiles of multiple gases were sampled from an aircraft on an approximately biweekly basis at four sites in the Amazon basin: Alta Floresta (ALF), Santarém (SAN), Rio Branco (RBA), and Tabatinga (TAB) (Figure 1). An extensive description of the methods and analysis of the observations are found in *Gatti et al.* [2014]. With the dominant wind direction being from the tropical Atlantic, the region of influence of the four sites covers a large fraction of the Amazon basin. In particular, samples from the two sites in the Western Amazon (TAB and RBA) include information about the carbon fluxes from a large part of the undisturbed rainforest, whereas the samples from the two other sites (ALF and SAN) are also partly influenced by savannah and agricultural land.

Besides the observations from the Amazon, we have used atmospheric CO_2 observations from the ObsPack data products provided by NOAA [*Masarie et al.*, 2014]. These ObsPacks include observations from a global network of monitoring stations. For this study we have used ObsPack version 1.0.4 [*ObsPack*, 2013]. In total we have used over 56,000 CO_2 observations measured by 13 different laboratories from 98 locations globally. An overview of these observations and sites is given in the supporting information. All CO_2 observations used in this study are on the same World Meteorological Organization CO_2 X2007 calibration scale.

The observations have been divided in different categories and assigned model-data mismatch values accordingly. This model-data mismatch defines how much weight is given to observations from a certain site. It represents the ability of our model to simulate the CO_2 concentrations at a given measurement site and thereby includes transport errors as well as errors related to the representativeness of the site for the grid box it is located in. We use the following model-data mismatch values for these eight categories: deep southern hemisphere (0.50 ppm), marine boundary layer (0.75 ppm), mixed (1.50 ppm), aircraft (2.00

ppm), land (2.50 ppm), tall tower (3.00 ppm), small tower (4.00 ppm), and problematic (5.00 ppm). As in *Peters et al.* [2007], these values represent subjective choices and are not based on an optimization or analysis of representation errors in our model. Sites were categorized to yield an innovation χ^2 close to 1.0 in each category.

Observations from non deep southern hemisphere and marine boundary layer sites are discarded from the assimilation when the simulated-minus-observed residuals exceed three times the assigned model-data mismatch.

2.5. State Vector and Covariance Structure

The linear scaling factors for the terrestrial biosphere and ocean carbon fluxes λ_r are optimized in CT-SAM on a weekly basis. CT-SAM uses a square-root ensemble Kalman filter [*Whitaker and Hamill*, 2002] with a smoother window length of 5 weeks, as in *Peters et al.* [2007]. For each of the 150 ensemble members, a set of scaling factors and CO_2 mole fractions are calculated [see also *Peters et al.*, 2005]. The prior estimates of λ_r for each given week are calculated as the mean of the optimized parameters from the two previous weeks and the fixed prior value of 1.0 (representing the unadjusted prior carbon fluxes).

The state vector in CT-SAM (i.e., the vector containing all parameters λ_r to be optimized) is based on *Peters et al.* [2007] but uses the biome type map of the SiBCASA model instead of the previously used Olson ecosystem classification system [*Olson et al.*, 1985]. For each of the nine TransCom land regions outside South America, one scaling factor is optimized for each of the 13 original SiBCASA ecoregions (i.e., biome types). Within South America, we optimize scaling factors for each $1° \times 1°$ grid box, rather than for each biome type.

The prior covariance structure describes the magnitude of the uncertainty on each scaling factor, as well as their correlation in space. Temporal correlations are not considered explicitly in our system. For each $1° \times 1°$ grid box within South America, the individual parameters are coupled with the spatial covariance structure calculated by

$$C = 0.64 \cdot \exp^{-d/L} \tag{2}$$

where d is the distance between the grid boxes and L is the length scale, for which we used 300 km. The underlying land cover map for South America is shown in Figure 1 and is used to calculate the prior covariance structure. To improve the representation of the spatial variability within the Amazon region, we further subdivided the original SiBCASA tropical forest biome (Tall Broadleaf-Evergreen Trees) into three different climate zones, based on the Köppen climate classification system [*Kottek et al.*, 2006]: Tropical Savannah, Tropical Monsoon, and Tropical Rainforest. The 30 ocean regions to be optimized have a covariance structure based directly on the calculations in the ocean inversion model [*Jacobson et al.*, 2007]. The chosen prior uncertainty is 80% on land parameters and 40% on ocean parameters.

Theoretically, this approach leads to a total of 1812 parameters to be optimized each week, but in practice, the number is smaller because not every ecoregion is represented in each TransCom region and certain regions, such as deserts and ice-covered regions, are not optimized. The number of degrees of freedom is about 409 each week, as calculated from singular value decomposition of the covariance matrix [*Patil et al.*, 2001; *Peters et al.*, 2005].

2.6. Optimizing SiBCASA-GFED4 Biomass Burning Emissions

As described before, in CT-SAM we impose the biomass burning emissions from a range of different modeled estimates. In a separate framework, we optimize one of those estimates, the SiBCASA-GFED4 biomass burning emissions, with the TM5-4DVAR system, as described by *Krol et al.* [2013], using a similar setup of the TM5 transport model [*Krol et al.*, 2005] (see supporting information). Emissions are optimized using CO flask observations and a large set of daytime total column CO observations over South America from the Infrared Atmospheric Sounding Interferometer (IASI) on board the METOP-A satellite [*Clerbaux et al.*, 2009]. The CO data were retrieved using the Fast Optimal Retrievals on Layers for IASI algorithm [*Hurtmans et al.*, 2012]. Besides the IASI observations, we also assimilate the surface flask CO observations from 36 sites of the NOAA ESRL Carbon Cycle Cooperative Global Air Sampling network [*Novelli and Masarie*, 2013] and, in one case, the CO observations from the Amazon aircraft profiles [*Gatti et al.*, 2014] as described in section 2.4.

Table 1. Overview of the Setups of the Different Inverse Experiments for CO_2

Case	Biomass Burning Emissions	CO_2 Observations Amazon
C1	SiBCASA-GFED4 optimized with IASI and Amazon data	Included
C2	SiBCASA-GFED4 optimized with IASI	Included
C3	SiBCASA-GFED4	Included
C4	GFAS	Included
C5	FINN	Included
C6	SiBCASA-GFED4	Excluded

The prior emissions of the TM5-4DVAR system are split in three categories: (1) biomass burning emissions, optimized in 3 day periods, (2) atmospheric oxidation of nonmethane hydrocarbons, optimized on a monthly time resolution, and (3) anthropogenic emissions (not optimized within South America). We have used the biome-specific emission factors from the GFED-A&M [*Andreae and Merlet*, 2001] scenario from *van Leeuwen et al.* [2013] to obtain the prior biomass burning CO emissions from SiBCASA-GFED4. After the optimization of the biomass burning emissions using CO, we derived biomass burning CO_2 emissions by applying the same percentage of change between the prior and the optimized fluxes as found for CO to the CO_2 emissions for each $1°\times1°$ degree grid box in South America. As in *Krol et al.* [2013] our system only scales the prior biomass burning CO emissions, and it is therefore not possible to assign biomass burning CO emissions to areas with no emissions in the prior. More details are given in the supporting information.

2.7. Inverse Experiments

We performed a suite of atmospheric inversions to get a range of estimates for the Amazon carbon balance (see Table 1). In all experiments we use the same state vector (section 2.5) and TM5 setup (section 2.3). In C1 and C2 we use the biomass burning emissions optimized with satellite-observed CO columns (section 2.6). C1 also included the CO observations from the Amazon aircraft profiles in the biomass burning optimization. The biomass burning emissions in C3 are the original SiBCASA-GFED4 emissions before optimization with CO observations. C4 and C5 use GFAS and FINN biomass burning emissions, respectively. The final experiment C6 is as C3 using SiBCASA-GFED4 but did not include CO_2 observations from the Amazon aircraft profiles in the CO_2 flux optimization.

3. Results

3.1. Biomass Burning Emissions

The annual mean carbon balance of the Amazon is strongly controlled by CO_2 emissions from fires, which vary strongly from year to year. Figure 2 shows the daily fire CO_2 emissions for 2010–2011 with peaks during August–October each year. The emissions in the 2010 dry season (July–October) clearly exceed those in the 2011 dry season in all estimates. In the nonoptimized emission estimates, the difference between 2011 and 2010 is 0.16 PgC/yr (GFAS), 0.24 PgC/yr (FINN), and 0.43 PgC/yr (SiBCASA-GFED4), in comparison to 0.21 PgC/yr from *Gatti et al.* [2014] (Table 4). In comparison to previous years (not shown), the biomass burning anomaly in the drought year 2010 is marked by a much larger peak of emissions in the dry season. This 2010 anomaly is largest for SiBCASA-GFED4, where biomass burning peaks earlier in the dry season with much larger emissions compared to the other products.

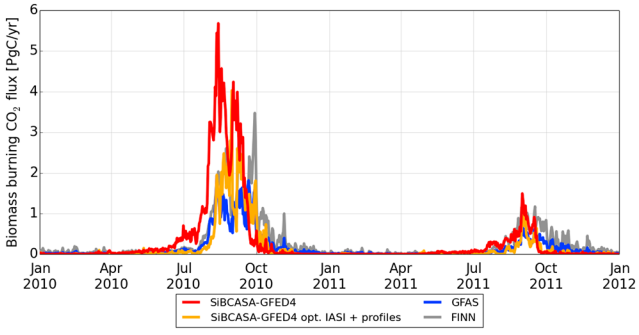

Figure 2. Daily biomass burning CO_2 emissions for the Amazon for four biomass burning products: the SiBCASA-GFED4 prior, the optimized fires with CO from IASI and profiles, and the GFAS and FINN inventories for the years 2010 and 2011.

When we additionally use satellite-observed CO columns from IASI and the Amazon profile measurements to optimize fire emission strengths from SiBCASA-GFED4, the peak emissions shift to later in the dry season and are

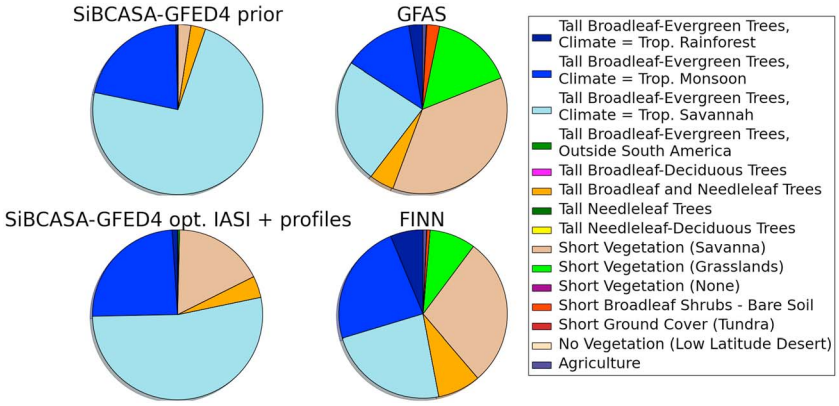

Figure 3. Biomass burning CO_2 emissions per biome type in the Amazon region for the SiBCASA-GFED4 prior, the optimized fires with IASI, and the GFAS and FINN inventories for the years 2010 and 2011.

smaller. The two cases where we either do or do not assimilate Amazon CO observations besides IASI CO observations give very similar results, and we therefore do not show them separately in the figures. Optimizing the SiBCASA-GFED4 emissions brings them in better agreement with GFAS and FINN, but the emissions from FINN occur later in the biomass burning season than the other estimates. The annual mean CO_2 emissions for 2010 from the optimized biomass burning estimate are close to half (0.27 PgC/yr) of the original SiBCASA-GFED4 estimate (0.53 PgC/yr) and agrees more closely with GFAS. However, the reduced emissions are no longer in agreement with the *Gatti et al.* [2014] estimate (0.51 PgC/yr) that agreed with the higher 2010 emissions of SiBCASA-GFED4. The FINN annual mean estimate of the 2010 CO_2 emissions (0.43 PgC/yr) lies between the estimates of Gatti/GFED4 and IASI/GFAS. We will show below (section 3.2) that the optimized SiBCASA-GFED4 emissions in general lead to a better correspondence to the atmospheric CO observations from *Gatti et al.* [2014] than the original SiBCASA-GFED4 emissions, the GFAS emissions, and the FINN emissions.

The change in biomass burning CO_2 emissions between the original SiBCASA-GFED4 estimate and the optimized results using CO consists of a spatial shift in emissions from the Amazon tropical forests to the more southward located savanna-dominated areas. Figure 3 shows that this change also makes the optimized emissions per land use type more consistent with GFAS and FINN, with burning in the Brazilian Cerrado (Savannahs and Grasslands) accounting for 25–50% of the total carbon emissions. The Cerrado typically has a smaller fuel load and lower emissions of CO per kg dry matter burned (60–80 g kg^{-1} DM) than tropical forests (100 g kg^{-1} DM). This spatial shift of emissions to the Cerrado thus simultaneously reduces both CO and CO_2 emissions, as well as their emission ratio. To see which signals drive this shift, we next turn to the atmospheric mole fractions of CO and CO_2.

3.2. Atmospheric CO Observations

The optimization of the SiBCASA-GFED4 biomass burning emissions with TM5-4DVAR CO system typically increases the amount of CO in the atmosphere during the wet season in both 2010 and 2011, while dry season CO is reduced. The IASI CO columns strongly drive these emission changes, and a general good correspondence with data is obtained after optimization. This is illustrated in column CO values for a specific day in the 2010 dry season in Figure 4. This improvement is achieved by (a) a reduction of CO emissions from the Amazon, most notably in 2010, and (b) an increase of the global background CO mole fractions by close to 30 ppb. The latter change is driven by the assimilation of the NOAA background CO observations. This shift in background CO also makes the simulations more consistent with the observed CO surface time series at background sites around continental South America, such as Tierra Del Fuego, Ushuaia, Argentina (TDF), Ragged Point, Barbados (RPB) and Ascension Island, UK (ASC). The latter two were used in *Gatti et al.* [2014] to define inflow conditions against which to analyze the excess CO from selected observed profiles, and matching these sites in our model is a prerequisite to correctly attribute regional CO enhancements to regional fire emissions too.

Besides the inversions using CO observations from IASI (F2) and additional Amazon profile observations (F1), we have performed forward simulations using the biomass burning products: SiBCASA-GFED4 (F3), GFAS (F4),

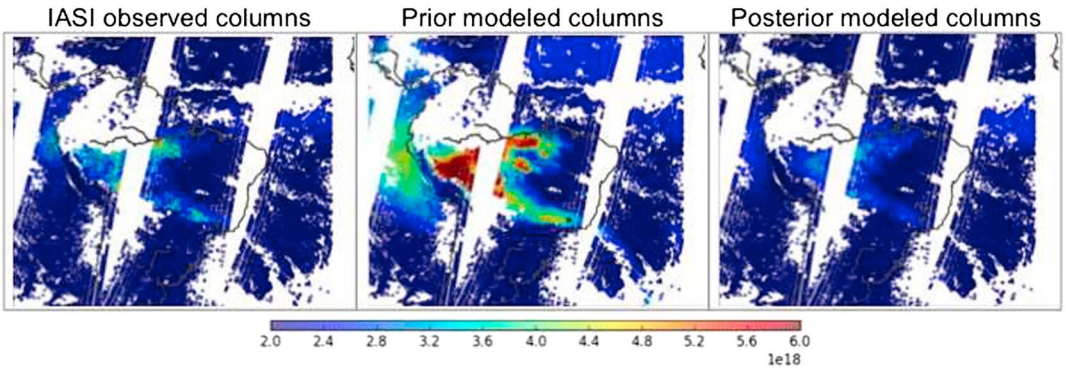

Figure 4. CO columns (molecules cm^{-2}) measured over South America on 14 August 2010 by (left) IASI and modeled with (middle) prior SiBCASA-GFED4 emissions, and (right) optimized SiBCASA-GFED4 emissions.

and FINN (F5). For F3–F5 we use the optimized background CO for the rest of the world from the IASI inversion (F1). Figure 5 shows the comparison of the modeled and observed vertical profiles of the CO mole fractions at the four aircraft sites in the Amazon. For each site we show the median values at each vertical level over one of the four seasons included in our study [2010, 2011 wet (November–June) or dry (July–October) season]. The CO signal from biomass burning is visible by the higher mole fractions in the dry seasons. The figure shows how the optimized fires generally lead to a better agreement with the observed CO profiles at the four Amazon sites. The root mean square differences (RMSD) are given in Table 2 for each of the simulations with the different biomass burning products. Note that for F2, this presents an independent comparison, as the CO profiles were not used in the optimization. Over forests,

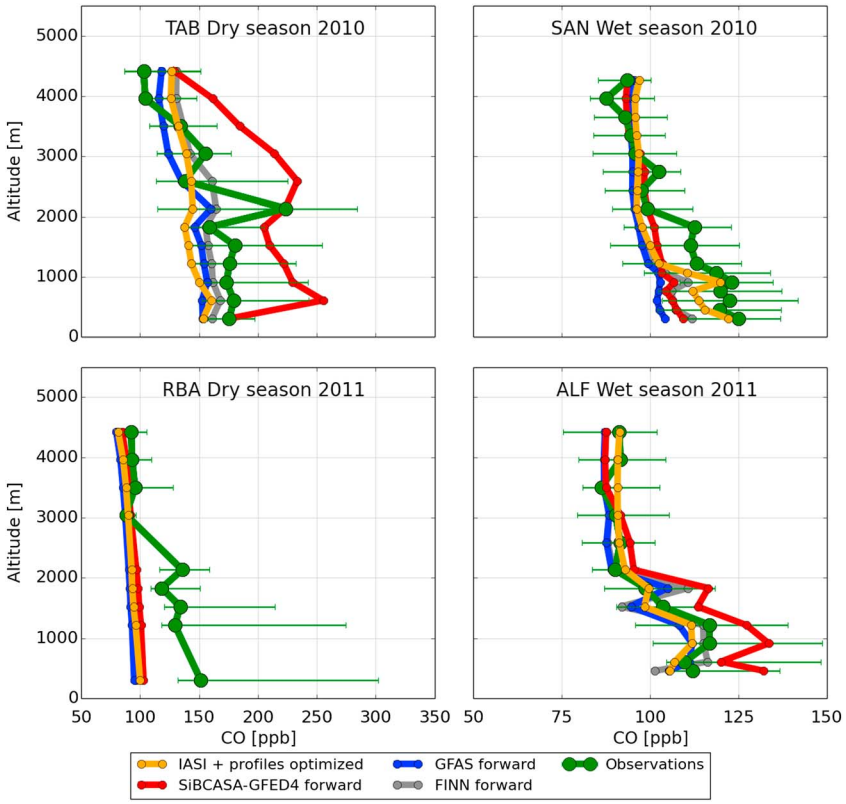

Figure 5. Comparison of the modeled CO mole fractions to the Amazon profiles for forward simulations of four of the biomass burning products. Examples are shown for each site for the median of either the 2010 or 2011 wet or dry season. The error bars are given for the 25th and 75th percentiles, representing the temporal variation. Note the different *x* axes for wet and dry seasons.

Table 2. Root Mean Square Differences (RMSD) Between Observed and Simulated CO Mole Fractions for 2010 and 2011 [ppb][a]

		ALF	RBA	SAN	TAB	RPB	ASC	TDF
F1	Optimized with IASI and profiles	**38**	**42**	**20**	52	24	23	8
F2	Optimized with IASI	41	53	29	53	24	23	8
F3	SiBCASA-GFED4 (prior)	74	110	32	71	24	23	8
F4	GFAS	50	56	28	47	24	22	8
F5	FINN	45	64	25	**42**	24	22	8

[a]Lowest RMSD per site are indicated in bold.

IASI is generally sensitive to altitudes above the 5 km ceiling of the unpressurized Amazonia flights. The improved RMSD from F3 to F2 shows that the optimization using IASI observations alone brings the simulated mole fractions into much better agreement with the Amazon profile observations than the prior. The forward simulations with GFAS (F4), FINN (F5), and the original SiBCASA-GFED4 (F3) fire emissions are also independent of the Amazon observations. The use of the same optimized background is visible in the same RMSD at the locations outside the area of the biomass burning emissions. F1 reaches the overall lowest RMSD versus the Amazon CO profile observations, profiting from both the IASI columns and CO profiles that were ingested. We note though that in F1, the IASI profiles are a much stronger constraint than the profile data simply because of the much higher volume of data from IASI. Finally, we see the much better performance (in terms of RMSD) of F1 and F2, compared to F3, as further evidence that SiBCASA-GFED4 fire emission estimates are likely too high.

3.3. Atmospheric CO_2 Observations

The next step in our approach is to use the different biomass burning products in the CO_2 inversions (recall Table 1) in which we optimize the net biome CO_2 exchange (NBE) while keeping the biomass burning emissions fixed. Table 3 presents the RMSD for the optimized CO_2 mole fractions of the different cases, together with the results from the forward simulation of the SiBCASA-GFED4 prior. A comparison between the simulated and observed CO_2 profiles is shown in Figure 6. When we look at the CO_2 mole fractions, we find the lowest overall RMSD at the four Amazon sites for the optimized fire simulation (C1). Especially in the dry season the adjustments to the simulated profiles are large (3–5 ppm), while the wet season adjustments are more modest (1 ppm). The adjustments are not simply a linear scaling of the a priori profile but show a vertical structure that suggests the influence from biomass burning emissions and biospheric CO_2 exchange manifest themselves at different altitudes and times. Examples are the profiles at TAB (2010 dry season) and RBA (2010 wet season), where the vertical gradient of CO_2 is changed after optimization, in better agreement with the observations.

As expected, the worst performance against the Amazonian profiles is seen when we optimize surface fluxes while only using observations from non-Amazonian sites (C6). Interestingly, the RMSD are even larger than in a forward simulation of the prior SiBCASA-GFED4 fluxes. In absence of direct constraints, the tropical fluxes then seem to become a residual for fluxes needed to balance the carbon budget of more distant regions, such as the Northern Hemisphere extratropics. This behavior in inversions has been described before and was hypothesized to explain the typical dipole behavior of the estimated Northern Hemisphere and

Table 3. RMSD Between Observed and Simulated CO_2 Mole Fractions for 2010 and 2011 [ppm][a]

	ALF	RBA	SAN	TAB	RPB	ASC	TDF
SiBCASA-GFED4 (prior)	3.02	3.30	2.38	3.19	1.13	0.90	0.56
C1 (IASI + Amazon)	**1.86**	**1.98**	1.46	2.27	0.75	0.56	0.46
C2 (IASI)	2.21	2.04	1.63	2.15	**0.69**	**0.55**	0.48
C3 (GFED4)	2.11	2.35	1.30	2.18	0.73	0.56	0.46
C4 (GFAS)	2.88	2.06	**1.27**	2.34	0.75	0.57	**0.43**
C5 (FINN)	2.20	2.14	1.28	**2.06**	0.76	0.57	0.46
C6 (excl. Amazon)	3.50	4.86	1.35	3.82	0.74	0.60	0.50

[a]Lowest RMSD per site are indicated in bold.

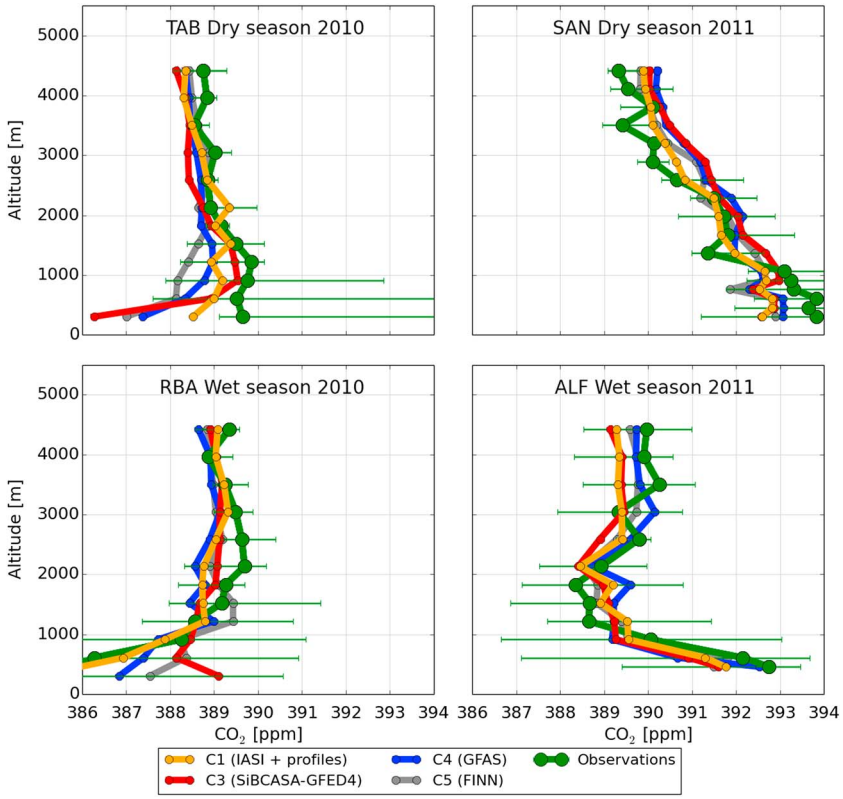

Figure 6. Comparison of the modeled CO_2 mole fractions to the Amazon profiles for four of the cases of inverse experiments. Examples are shown of each site for the median of either the 2010 or 2011 wet or dry season. The error bars are given for the 25th and 75th percentiles, representing the temporal variation.

tropical fluxes [*Stephens et al.*, 2007]. In our setup we use an ensemble Kalman filter with a smoother window of 5 weeks, and observations further downstream than those 5 weeks will therefore not influence our Amazon fluxes. Longer window lengths would allow the Amazon fluxes to be constrained by nonlocal observations. However, simulations with different window lengths have shown that this indeed not only gives a better match to the observations in remote places but also gives a larger projection of residual fluxes in regions such as the Amazon, but also in Africa, Asia, and Australia [*Babenhauserheide et al.*, 2015]. The results of C6 therefore strongly caution against interpreting Amazonian carbon surface fluxes without any regional observations to anchor the estimate. It moreover shows the large value of the Amazonian airborne observation program and its potential to inform us on the behavior of the regional carbon balance.

Table 4. Amazon Carbon Budget for 2010 and 2011, Separated in Biomass Burning (Fire) and Net Biome Exchange (NBE) [PgC/yr][a]

	Fire		NBE		Total		
	2010	2011	2010	2011	2010	2011	% NBE
Gatti et al. [2014]	+0.51	+0.30	−0.03	−0.25	+0.48 ± 0.18	+0.06 ± 0.10	52
C1 (IASI + Amazon)	+0.27	+0.05	−0.20	−0.32	+0.07 ± 0.42	−0.27 ± 0.42	35
C2 (IASI)	+0.27	+0.05	−0.15	−0.26	+0.12 ± 0.41	−0.21 ± 0.43	33
C3 (GFED4)	+0.53	+0.10	−0.40	−0.34	+0.13 ± 0.42	−0.24 ± 0.42	−16
C4 (GFAS)	+0.24	+0.08	−0.15	−0.23	+0.09 ± 0.41	−0.15 ± 0.42	33
C5 (FINN)	+0.41	+0.17	−0.10	−0.36	+0.31 ± 0.42	−0.19 ± 0.42	52
C6 (excl. Amazon)	+0.53	+0.10	−0.23	−0.43	+0.30 ± 0.49	−0.33 ± 0.46	32
SiBCASA-GFED4 (not optimized)	+0.53	+0.10	−0.40	−0.40	+0.14	−0.30	0

[a]The total budget (fire + NBE) is also included as is the percentage of the difference of the total CO_2 flux between both years represented by the biosphere (% NBE).

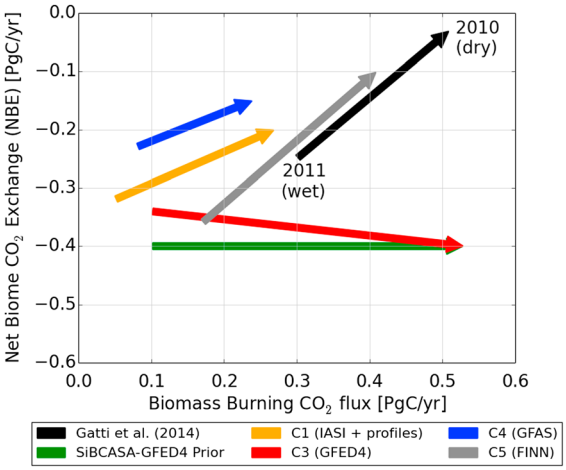

Figure 7. Drought response of the Amazon net biome CO_2 exchange (NBE) and biomass burning CO_2 fluxes between 2010 and 2011 for several cases. The start of the arrows represent 2011 (wet year), and the end represents 2010 (dry year).

3.4. Amazon Carbon Balance 2010–2011

Our estimates from cases C1 through C5 suggest that the Amazonian carbon balance for 2010 resulted in a net source of between $+0.07 \pm 0.42$ and $+0.31 \pm 0.42$ PgC/yr, while the net balance for 2011 was a sink of -0.15 ± 0.42 to -0.27 ± 0.42 PgC/yr (Table 4). The difference between both years amounts to 0.24–0.50 PgC/yr increase in the total net carbon release in the drought year 2010 relative to 2011. This is in most cases somewhat smaller than the estimate of *Gatti et al.* [2014] who report a total increase of carbon release of 0.42 ± 0.21 PgC/yr between the same years. This smaller estimate of the difference coincides with smaller absolute biomass burning emission estimates for both CO and CO_2 in our method compared to *Gatti et al.* [2014], and we speculate this might be related to vertical transport as will be discussed in section 4. Note that the estimated annual mean uncertainty on each individual inversion is an upper limit, given that the CT-SAM system does not propagate flux uncertainty beyond its 5 week window. As argued previously [*Peylin et al.*, 2005; *Peters et al.*, 2007] the representation of the uncertainty estimate as a range of results from alternative realizations of the inverse problem complements the formal annual Gaussian uncertainty estimate derived from the covariance matrix. Using our range of estimates as a measure for our uncertainty, our results are significantly different from those found by *Gatti et al.* [2014].

Figure 7 shows the drought response of NBE and biomass burning between 2010 and 2011 for the different cases. The figure shows (on the *x* axis) that the SiBCASA-GFED4 prior has high biomass burning emissions in 2010 and also a large difference between both years. These biomass burning emissions are used in C3 where the net CO_2 flux (NBE + biomass burning) is optimized using the global network of CO_2 observations. Since the biomass burning emissions are imposed to be these high values and the total net flux is optimized, the resulting biosphere response in C3 is small. The optimized NBE in C3 therefore stays close to the prior NBE of SiBCASA-GFED4, and we even find an unlikely slightly higher uptake in 2010 compared to 2011, which is opposite of what was found for the other cases. Therefore, C3 is not taken into account in the remainder of this section. The other cases show similar patterns in reduction of the NBE from 2010 to 2011 in combination with lower biomass burning emissions in the wet year 2011. The size of the fluxes and the difference corresponds well between optimizations with IASI and with GFAS fire emissions. Optimization with FINN fires yields results closest to *Gatti et al.* [2014].

Of the total reduction in uptake in 2010, we attribute about 34% (C1, C2, and C4) or 52% (C5) to reduced carbon uptake by the terrestrial biosphere, compared to the 52% estimated by *Gatti et al.* [2014]. The absolute reduction in biospheric carbon uptake during the 2010 drought in our estimates is 0.08 to 0.26 PgC/yr, which is larger than the prior estimate from the SiBCASA-GFED4 model (0.0 PgC/yr) but generally smaller than the *Gatti et al.* [2014] estimate (0.22 PgC/yr). Our expanded analysis thus finds a smaller sensitivity of the tropical biosphere to droughts than the original interpretation of the profile data by *Gatti et al.* [2014], as we will discuss further in section 4.

Figure 8 shows the seasonal patterns of NBE for the different cases. The majority of the biospheric carbon uptake occurs in the July–September period, a large part of the dry season. Biospheric carbon uptake in our SiBCASA model typically peaks in the dry season as vegetation takes advantage of the available fPAR during cloudless conditions, as long as their deep roots can tap into the available soil water as implemented by *Harper et al.* [2010]. The cumulative difference in NBE between the drought year 2010 and the wet year 2011 is shown in Figure 8. The figure shows that the anomaly in uptake is mainly accumulated in the months after the dry season during which most of the biomass burning occurs. The

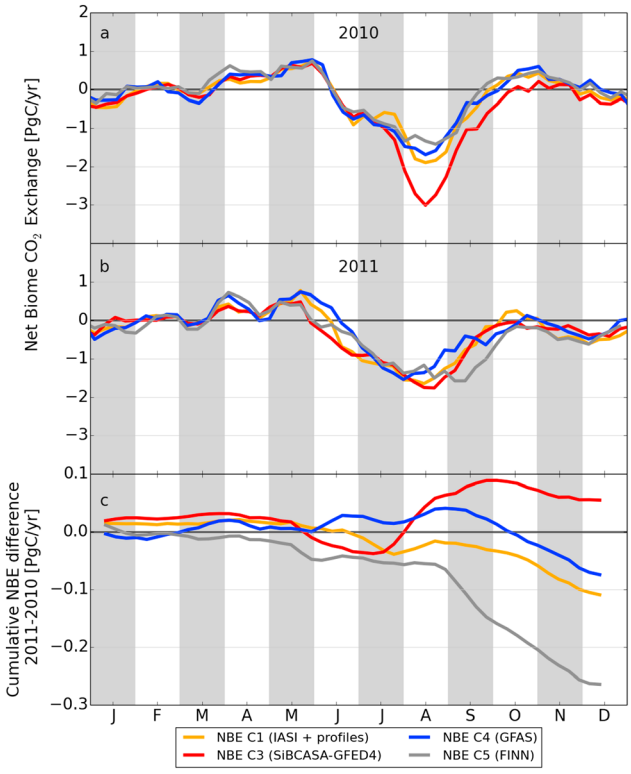

Figure 8. Time series of Amazon net biome CO_2 exchange (NBE) for (a) 2010, (b) 2011, and (c) the cumulative difference between 2010 and 2011 for four of the inversion cases.

response of the biosphere to the additional fire stress in 2010 leads to a lower biospheric uptake in the post-fire season.

4. Discussion

We have presented the Amazon carbon balance estimates from our CT-SAM system. This balance is dominated by biomass burning emissions that account for about 50–65% of difference in the total net carbon flux between 2010 and 2011. We have explored a range of emission estimates based on different biomass burning models, which gives new information on the resulting biospheric response to the 2010 drought. Our findings are generally in line with previous estimates for both the annual mean balance and the drought impact of 2010, such as those from *Gatti et al.* [2014], *Phillips and Lewis* [2014] and *Pan et al.* [2011]. CT-SAM not only allows for a large scale evaluation of the integrated carbon fluxes but also gives a detailed picture of the spatial variability and distribution over different biomes.

In section 3.4 we focused on the change in the fluxes between 2010 and 2011 and compared the drought response of our simulations to the results of *Gatti et al.* [2014]. The net fluxes estimated by inverse models are generally less robust than the interannual variability [*Baker et al.*, 2006]. Although less robust, we find from our simulations a smaller net source of carbon in 2010 than *Gatti et al.* [2014] and in 2011 we find a net sink of carbon, whereas *Gatti et al.* [2014] find a small net source. The year 2010 was a drought year, and follow-up research spanning 2010–2014 will tell us whether 2011 can be considered an average year, or a year with especially large uptake as a recovery effect after the drought or due to especially wet and warm conditions. A new study of Alden et al. (submitted manuscript, 2015) shows the results of regional inversions of the Amazon region, showing that our NBE estimates are on the high uptake side of the range of this multi-model ensemble. The biomass burning estimate for 2011 from *Gatti et al.* [2014] is high in comparison to the other estimates, which could be due to the use of the CO:CO_2 ratio from 2010 to calculate 2011 emissions, and the potential underestimation of the dry season biogenic CO flux on the total CO flux.

The main differences between our method and that used in *Gatti et al.* [2014] include the horizontal transport, vertical transport, prior assumptions, and the use of an implicit or explicit background. Transport in *Gatti et al.* [2014] was based on backtrajectories from a Lagrangian particle dispersion model (Hysplit) and is based on column integral differences, thereby not making any assumptions on the vertical transport in the lower troposphere. In contrast, our method aims to vertically resolve the profile data and therefore depends strongly on how well transport in general and vertical transport in particular is represented in our model. The *Gatti et al.* [2014] method, however, assumes that the signals from the surface fluxes only extend up to 4.5 km, the height up to which the measurements are made, whereas our approach allows the signal to propagate beyond that. Another difference is that our Bayesian method depends on the prior flux estimates together with their prior uncertainties, balanced with the observations and their assigned uncertainties. Finally, the method used in *Gatti et al.* [2014] forces the background to be a linear combination of the CO_2 concentrations at RPB and ASC, based on SF_6 [*Miller et al.*, 2007]. In contrast, the

background in CT-SAM is not explicitly forced as it is part of the global inversion. Large biases at those locations could lead also to biases in the resulting flux estimates. Examining the residuals at RPB and ASC (shown for C1 in Figures S6 and S7 of the supporting information) shows that the biases between our modeled and the observed CO_2 concentrations at those sites are low (maximum −0.34 ppm at RPB between November and April).

As stated by *Stephens et al.* [2007], the main uncertainties in the global carbon balance are in the tropics, where constraints from observations are sparse. The results from our case C6, where we optimize without including the Amazon profiles, highlight the importance of these data sets. Without the constraints from these profiles included in CT-SAM, the biospheric uptake is larger than for all other cases, and the prior is adjusted to a lesser degree. Also, the match to CO_2 observations becomes even worse than the results from a forward transport of the prior fluxes (Table 3). Observations in this region of high biospheric productivity and large biomass burning emissions are clearly important, also in constraining the fluxes on the global scale. The same likely holds for other tropical regions, such as Africa or Asia, where observations are also scarce.

We have compared our modeled mole fractions to the observed mole fractions from the aircraft flask samples for CO in section 3.2 and CO_2 in section 3.3. The medians of the seasonal vertical structure of the observed CO and CO_2 profiles were shown, together with the medians of the modeled CO and CO_2 profiles. The vertical profile is highly dependent on vertical transport and the convection scheme used in the transport model. In our cases presented in section 3.4, we used an updated convection scheme in TM5 using the convection fields from ECMWF directly (see section 2.3). We have also studied the use of a convection scheme previously used in TM5 [*Tiedtke*, 1989]. The RMSD between the simulated and observed CO_2 mole fractions was larger for three out of four Amazon sites when using the Tiedtke convection scheme, based on which we decided to use the ECMWF convective fluxes in our presented inversions.

We presented the results from our two-step inverse approach, optimizing first CO fluxes from biomass burning emissions and second using those optimized fire estimates to optimize the NBE fluxes. As mentioned earlier, the CO inversion cannot assign biomass burning emissions to grid boxes with zero emission, thereby restricting the fluxes to the areas given in the prior estimate from SiBCASA-GFED4. The two inversions with IASI observations give very similar results for the optimized biomass burning emissions, showing that including the additional CO observations from the aircraft profiles adds only a small amount of information to that from the large number of IASI observations. Over forests, the IASI observations are mainly sensitive to higher altitudes, the peak sensitivity is between 4 and 6 km. The altitude below 5 km is mainly constrained by the biweekly Amazon profile observations. Large signals or plumes from specific (biomass burning) events could possibly be missed. Increasing the frequency of the measurements would therefore be valuable, especially in the dry season (the period with the largest fire emissions and NBE; see Figure 8.

The estimates of CO biomass burning used in section 3.1 could be sensitive to the vertical injection profile used in the CO inversions. In the supporting information we describe a set of experiments to test that sensitivity. The results are presented in Figure S3. The "Base" case presented there is comparable to the setup used in this work, whereas the other five are variations using different injection profiles and/or different day/night variations in the biomass burning emissions. Our experiments show that in the stronger biomass burning year, 2010, the choice of an injection profile and diurnal variations in the emissions makes less than 5 TgC difference out of 30 TgC. In 2011, the maximum impact is 3 TgC out of 5 TgC, and therefore lower in absolute sense, but higher when seen as a fraction of the emissions in that year. Using the 75 ppb CO/ppm CO_2 estimate used by *Gatti et al.* [2014], this yields a spread in the biomass burning CO_2 emission of 0.07 PgC in 2010 and 0.04 PgC in 2011, compared to 0.51 and 0.30 PgC estimates of *Gatti et al.* [2014], respectively. Thus, the choice of a realistic injection profile causes a relatively small error in the estimate of biomass burning CO. This conclusion, however, should not be taken as a general statement about the use of injection profiles in atmospheric CO modeling; rather, it is only valid in this case because (a) tropical South America is a region of deep convective mixing even in the absence of an explicit injection profile, and (b) we assimilate IASI total columns, which are sensitive primarily to CO above 4 km, i.e., above the top level of most injection profiles used. The picture could be totally different if, for example, the Amazonian aircraft profiles were assimilated and IASI CO columns were not.

Our modeled CO and CO_2 profiles fall outside the 25th–75th percentile range compared to the observations especially at the lower altitudes in the dry season. The update of the convection scheme used in TM5 improved our match to the observations but not more than e.g. using different biomass burning emissions. We showed above that the choice of different injection profiles did not change our final estimates strongly. Increased injection heights have a similar effect as enhanced mixing in the boundary layer. Possibly, improvement in vertical mixing specifically in the entrainment zone and cloud convective layers is needed [*Vilà-Guerau de Arellano*, 2014]. This could enhance the mixing of surface CO_2 fluxes to the free troposphere.

In our SiBCASA-GFED4 biosphere model, the Amazon NBE fluxes were equal in 2010 and 2011, showing no response to the drought. However, we do see a slight drought response in both GPP and respiration for the Amazon in the model. GPP is lower by 0.07 PgC/yr, which is balanced by an almost equal decrease in respiration of 0.08 PgC/yr. Our results could guide a better parameterization for droughts in the biosphere model. This is also concluded from a study on effects of droughts on water-use efficiency [*van der Velde*, 2015]. The deep rooting depth implementation in SiBCASA [*Harper et al.*, 2010] was based on comparison to observations at one location in the Amazon. The lack of drought response in our NBE fluxes suggests that this implementation might not be suitable for the entire Amazon basin. Additional observations from e.g. the RAINFOR network or satellite observations such as fluorescence could be used to improve the constraints for GPP and NPP.

The three products estimating biomass burning emissions have similar global emissions of CO and CO_2 but, as seen in section 3.1, show different behaviors on the continental and regional scales. The GFAS estimates are based on fire radiative power (FRP), which is combined with biome-specific conversion factors derived with regressions against GFED to calculate the amount of dry matter burned. FINN also relies on active fire observations to estimate burned areas and dry matter burned, rather than FRP. Both GFED and FINN use a similar approach to calculate the emissions that is based on information on the area burned, fuel load, and the burned fraction. FINN uses biome-averaged emission factors from *Akagi et al.* [2011], while GFED and GFAS rely on the compilation of *Andreae and Merlet* [2001]. One aspect leading to differences in these methods is the sensitivity of the three methods to relatively small fires. Also, the detection of fires underneath clouds and below the canopy is difficult in all three methods. Our approach to optimize the emissions using CO observations combines the strengths of the emission products with local observations.

A somewhat independent metric we can use to evaluate our system is the observed CO:CO_2 mole fraction ratio of the Amazon profile observations. As we use a two-step approach with CO and CO_2 in two separate inversions, their ratio is not directly used as an observational constraint, as would have been the case in a joint inverse system. The CO:CO_2 ratio in the atmosphere gives information on the type and amount of biomass burning emissions at the surface and is used by *Gatti et al.* [2014] to calculate the contribution of fires to the obtained fluxes. We have calculated the CO:CO_2 ratio for the simulated mole fractions of our four cases and compared it to the observed ratios for the four sites. For this, we used the enhancement of dry season profiles compared to background values of the wet season. The observed CO:CO_2 ratios are 76 ppb/ppm for Alta Floresta, 97 ppb/ppm for Santarém, 92 ppb/ppm for Rio Branco, and 172 ppb/ppm for Tabatinga. The difference between the modeled and observed ratio is generally smallest for the CO-optimized emissions (C1/F1) and FINN (C5/F5), followed by GFAS (C4/F4), while the largest deviations are found for GFED4 (C3/F3). This confirms our findings in section 3.4, where we found that the results from the inversion using GFED4 emissions yielded the least likely scenario for the drought response.

Our results focus on the comparison of different estimates for the Amazon carbon budget. The specific area defined as Amazon in our study, as shown in Figure 1, is an important factor in our analysis, especially when comparing to the results from *Gatti et al.* [2014]. We have therefore adopted the same definition of the area as used in their analysis. However, the observations from the flask profiles are of course influenced by processes outside this domain. The method used by *Gatti et al.* [2014] distributes the observed differences to the background values at the Atlantic coast and projects the calculated fluxes onto the whole column and the area defined as Amazon. However, the Sertão, encompassing the semi-arid regions of Northeastern Brazil, is also a region with large fluxes, even though the amount of biomass is much lower than in the Amazon. Our method allows for a separate estimate of the fluxes in the Sertão. Maps of the mean biomass burning and NBE fluxes are given for the different cases in Figures S4 and S5. When we extend our region toward

the east and include the Sertão in our analysis, we find higher biomass burning emissions, but the extent to which they increase varies per case. Additional biomass burning emissions from the Sertão are smallest for FINN (+7% for 2010 and +12% for 2011) and largest for GFAS (+25% for 2010 and +38% in 2011). For GFED4 (C3) and the emissions optimized using CO observations (C1 and C2), the emissions increase with values ranging between 15% and 26%. The effect on the NBE is much larger, and the changes are different between both years. Biospheric uptake of the combined Amazon and Sertão region is lower in all cases in 2010, totaling to even a small net source of NBE for C5. In 2011, the Sertão adds the opposite effect, and the biospheric sink of the combined region is larger with values up to 65% than from the Amazon region alone. The effects for both years combine into a larger difference in both years, especially by the stronger biospheric drought response in the Sertão. In section 3.4, we found a smaller sensitivity to the effects of the drought in the Amazon than *Gatti et al.* [2014], but we show here that the area over which the fluxes are integrated is important to correctly estimate the biospheric drought response.

5. Conclusions

We have set up a new version of the CarbonTracker data assimilation system focusing on South America, particularly the Amazon. We have used different biomass burning emission estimates, resulting in a range of estimates of the Amazon carbon budget. Across our range of alternative inversions, we find the Amazon to be a net sink of carbon in 2011 and a net source in 2010.

We have optimized SiBCASA-GFED4 biomass burning emissions using IASI satellite CO observations and Amazon aircraft profile measurements of CO. These optimized emissions and the estimates from GFAS and FINN show that the start of the biomass burning season is later in the year than the original estimate from SiBCASA-GFED4. In comparison to this original SiBCASA-GFED4 estimate, our optimized emissions are in better agreement particularly with the GFAS estimate. We estimate the 2010–2011 difference in biomass burning emissions to be between 0.16 and 0.24 PgC/yr.

Starting from the different imposed biomass burning emissions, we estimate the biospheric response to the 2010 drought in the Amazon to amount to 0.08 to 0.26 PgC/yr less uptake. The range is determined from the set of alternative inversions using the different biomass burning estimates and represents the estimated uncertainty. The major part of the biospheric response to the drought is not restricted to the burning season but lasts during the post biomass burning period, September–December. The total drought response in the Amazon in our estimates is distributed between additional biomass burning and reduced uptake (NBE). The percentage to be ascribed to the reduction in NBE is, in most of our cases, around 35%, except for C5 (FINN) where the biospheric response accounts for 52%.

Acknowledgments

The authors would like to thank the contributing laboratories to the ObsPack data product prototype version 1.0.4 for their efforts in performing the high precision atmospheric CO_2 measurements at the various locations worldwide. We would specifically like to thank the contributing persons from the following laboratories of which we have assimilated the CO_2 observations in CT-SAM: Insituto de Pesquisas Energeticas e Nucleares (IPEN, Brazil), NOAA Earth System Research Laboratory (U.S.A.), Environment Canada (Canada), Commonwealth Scientific and Industrial Research Organization (Australia), Laboratoire des Sciences du Climat et de l'Environnement (LSCE, France) and the RAMCES team (Réseau Atmosphérique de Mesure des Composés à Effet de Serre, France), National Center For Atmospheric Research (U.S.A.), University of Bern (Switzerland), Lawrence Berkeley National Laboratory (U.S.A.), Scripps Institution of Oceanography (U.S.A.), University of Groningen (the Netherlands), Finnish Meteorological Institute (Finland), Meteorological State Agency of Spain (Spain), and the Hungarian Meteorological Service (Hungary). Observations collected in the U.S. Southern Great Plains (SGP) were supported by the Office of Biological and Environmental Research of the US Department of Energy under contract DE-AC02-05CH11231 as part of the Atmospheric Radiation Measurement Program (ARM). The biomass burning data used for this study are available from the GFED4 (http://www.globalfiredata.org), GFASv1 (https://www.gmes-atmosphere.eu/fire/), and FINNv1 (http://bai.acd.ucar.edu/Data/fire/) databases. IASI was developed and built under the responsibility of Centre National d'Etudes Spatiales (CNES) and flies onboard the MetOp satellite as part of the Eumetsat Polar system. The authors acknowledge the Ether French atmospheric database (http://ether.ipsl.jussieu.fr) for distributing the IASI L1C and L2-CO data. SiBCASA and CarbonTracker model results as presented in this paper are available upon request (ingrid.vanderlaan@wur.nl). This research has been financially supported by the GEOCARBON project (EU FP7 grant agreement: 283080) and a grant for computing time (SH-060-13) from the Netherlands Organization for Scientific Research (NWO). J.W. Kaiser is funded by the MACC-III project (EU H2020 grant agreement 633080). We furthermore acknowledge the AMAZONICA NERC grant NE/F005806/1 which funded a substantial part of the greenhouse gas measurements over the Amazon used in this paper. The authors would like to thank two anonymous reviewers for their comments.

References

Akagi, S. K., R. J. Yokelson, C. Wiedinmyer, M. J. Alvarado, J. S. Reid, T. Karl, J. D. Crounse, and P. O. Wennberg (2011), Emission factors for open and domestic biomass burning for use in atmospheric models, *Atmos. Chem. Phys.*, *11*(9), 4039–4072, doi:10.5194/acp-11-4039-2011.

Andreae, M. O., and P. Merlet (2001), Emission of trace gases and aerosols from biomass burning, *Global Biogeochem. Cycles*, *15*(4), 955–966, doi:10.1029/2000GB001382.

Araujo, A. C., et al. (2002), Comparative measurements of carbon dioxide fluxes from two nearby towers in a central Amazonian rainforest: The Manaus LBA site, *J. Geophys. Res.*, *107*(D20), 8090, doi:10.1029/2001JD000676.

Babenhauserheide, A., S. Basu, S. Houweling, W. Peters, and A. Butz (2015), Comparing the CarbonTracker and TM5-4DVar data assimilation systems for CO_2 surface flux inversions, *Atmos. Chem. Phys. Discuss.*, *15*, 8883–8932, doi:10.5194/acpd-15-8883-2015.

Baker, D. F., et al. (2006), TransCom 3 inversion intercomparison: Impact of transport model errors on the interannual variability of regional CO_2 fluxes, 1988–2003, *Global Biogeochem. Cycles*, *20*, GB1002, doi:10.1029/2004GB002439.

Booth, B. B. B., C. D. Jones, M. Collins, I. J. Totterdell, P. M. Cox, S. Sitch, C. Huntingford, R. A. Betts, G. R. Harris, and J. Lloyd (2012), High sensitivity of future global warming to land carbon cycle processes, *Environ. Res. Lett.*, *7*(2), 024002, doi:10.1088/1748-9326/7/2/024002.

Ciais, P., et al. (2013), Carbon and other biogeochemical cycles, in *Climate Change 2013: The Physical Science Basis. Contribution of Working Group I to the Fifth Assessment Report of the Intergovernmental Panel on Climate Change*, edited by T. F. Stocker et al., pp. 465–570, Cambridge Univ. Press, Cambridge, U. K., and New York.

Clerbaux, C., et al. (2009), Monitoring of atmospheric composition using the thermal infrared IASI/MetOp sounder, *Atmos. Chem. Phys.*, *9*(16), 6041–6054, doi:10.5194/acp-9-6041-2009.

Conway, T. J., P. P. Tans, L. S. Waterman, K. W. Thoning, D. R. Kitzis, K. A. Masarie, and N. Zhang (1994), Evidence for interannual variability of the carbon cycle from the National Oceanic and Atmospheric Administration/Climate Monitoring and Diagnostics Laboratory Global Air Sampling Network, *J. Geophys. Res.*, *99*(D11), 22,831–22,855, doi:10.1029/94JD01951.

Cox, P. M., D. Pearson, B. B. Booth, P. Friedlingstein, C. Huntingford, C. D. Jones, and C. M. Luke (2013), Sensitivity of tropical carbon to climate change constrained by carbon dioxide variability, *Nature*, *494*, 341–344, doi:10.1038/nature11882.

Dee, D. P., et al. (2011), The ERA-Interim reanalysis: Configuration and performance of the data assimilation system, *Q. J. R. Meteorol. Soc.*, *137*(656), 553–597, doi:10.1002/qj.828.

EDGAR4.2 (2011), Emission Database for Global Atmospheric Research (EDGAR), release version 4.2, European Commission, Joint Research Centre (JRC)/PBL Netherlands Environmental Assessment Agency. [Available at http://edgar.jrc.ec.europa.eu.]

Gatti, L. V., J. B. Miller, M. T. S. D'Amelio, A. Martinewski, L. S. Basso, M. E. Gloor, S. Wofsy, and P. Tans (2010), Vertical profiles of CO_2 above eastern Amazonia suggest a net carbon flux to the atmosphere and balanced biosphere between 2000 and 2009, *Tellus, Ser. B*, *62*(5), 581–594, doi:10.1111/j.1600-0889.2010.00484.x.

Gatti, L. V., et al. (2014), Drought sensitivity of Amazonian carbon balance revealed by atmospheric measurements, *Nature*, *506*(7486), 76–80, doi:10.1038/nature12957.

Giglio, L., J. T. Randerson, and G. R. Werf (2013), Analysis of daily, monthly, and annual burned area using the fourth-generation global fire emissions database (GFED4), *J. Geophys. Res. Biogeosci.*, *118*, 317–328, doi:10.1002/jgrg.20042.

Gloor, M., et al. (2012), The carbon balance of South America: A review of the status, decadal trends and main determinants, *Biogeosciences*, *9*(12), 5407–5430, doi:10.5194/bg-9-5407-2012.

Harper, A. B., A. S. Denning, I. T. Baker, M. D. Branson, L. Prihodko, and D. A. Randall (2010), Role of deep soil moisture in modulating climate in the Amazon rainforest, *Geophys. Res. Lett.*, *37*, L05802, doi:10.1029/2009GL042302.

Hurtmans, D., P.-F. Coheur, C. Wespes, L. Clarisse, O. Scharf, C. Clerbaux, J. Hadji-Lazaro, M. George, and S. Turquety (2012), FORLI radiative transfer and retrieval code for IASI, *J. Quant. Spectros. Radiat. Transfer*, *113*(11), 1391–1408, doi:10.1016/j.jqsrt.2012.02.036.

Jacobson, A. R., S. E. Mikaloff Fletcher, N. Gruber, J. L. Sarmiento, and M. Gloor (2007), A joint atmosphere-ocean inversion for surface fluxes of carbon dioxide: 1. Methods and global-scale fluxes, *Global Biogeochem. Cycles*, *21*, GB1019, doi:10.1029/2005GB002556.

Kaiser, J. W., et al. (2012), Biomass burning emissions estimated with a global fire assimilation system based on observed fire radiative power, *Biogeosciences*, *9*(1), 527–554, doi:10.5194/bg-9-527-2012.

Kottek, M., J. Grieser, C. Beck, B. Rudolf, and F. Rubel (2006), World map of the Köppen-Geiger climate classification updated, *Meteorol. Z.*, *15*(3), 259–263, doi:10.1127/0941-2948/2006/0130.

Krol, M., S. Houweling, B. Bregman, M. van den Broek, A. Segers, P. van Velthoven, W. Peters, F. Dentener, and P. Bergamaschi (2005), The two-way nested global chemistry-transport zoom model TM5: Algorithm and applications, *Atmos. Chem. Phys.*, *5*(2), 417–432, doi:10.5194/acp-5-417-2005.

Krol, M., et al. (2013), How much CO was emitted by the 2010 fires around Moscow?, *Atmos. Chem. Phys.*, *13*(9), 4737–4747, doi:10.5194/acp-13-4737-2013.

Kruijt, B., J. A. Elbers, C. von Randow, A. C. Araujo, P. J. Oliveira, A. Culf, A. O. Manzi, A. D. Nobre, P. Kabat, and E. J. Moors (2004), The robustness of eddy correlation fluxes for Amazon rain forest conditions, *Ecol. Appl.*, *14*(4 Supplement), S101–S113, doi:10.1890/02-6004.

Lee, J. E., et al. (2013), Forest productivity and water stress in Amazonia: Observations from GOSAT chlorophyll fluorescence, *Proc. R. Soc. B*, *280*(1761), 20130171, doi:10.1098/rspb.2013.0171.

Lewis, S. L., P. M. Brando, O. L. Phillips, G. M. F. Van Der Heijden, and D. Nepstad (2011), The 2010 Amazon drought, *Science*, *331*(6017), 554, doi:10.1126/science.1200807.

Malhi, Y., et al. (2002), An international network to monitor the structure, composition and dynamics of Amazonian forests (RAINFOR), *J. Veg. Sci.*, *13*(3), 439–450, doi:10.1111/j.1654-1103.2002.tb02068.x.

Malhi, Y., et al. (2006), The regional variation of aboveground live biomass in old-growth Amazonian forests, *Global Change Biol.*, *12*(7), 1107–1138, doi:10.1111/j.1365-2486.2006.01120.x.

Masarie, K. A., W. Peters, A. R. Jacobson, and P. P. Tans (2014), ObsPack: A framework for the preparation, delivery, and attribution of atmospheric greenhouse gas data, *Earth Syst. Sci. Data*, doi:10.5194/essd-6-375-2014.

Miller, J. B., L. V. Gatti, M. T. d'Amelio, A. M. Crotwell, E. J. Dlugokencky, P. Bakwin, P. Artaxo, and P. P. Tans (2007), Airborne measurements indicate large methane emissions from the eastern Amazon basin, *Geophys. Res. Lett.*, *34*, L10809, doi:10.1029/2006GL029213.

Nisbet, E. G., E. J. Dlugokencky, and P. Bousquet (2014), Methane on the rise—Again, *Science*, *343*(6170), 493–495, doi:10.1126/science.1247828.

Novelli, P. C., and K. Masarie (2013), Atmospheric carbon monoxide dry air mole fractions from the NOAA ESRL Carbon Cycle Cooperative Global Air Sampling Network, version: 2013-12-06. [Available at ftp://aftp.cmdl.noaa.gov/data/trace_gases/co/flask/surface/.]

ObsPack (2013), Cooperative Global Atmospheric Data Integration Project, Multi-laboratory compilation of atmospheric carbon dioxide data for the period 2000–2012 (obspack_co2_1_PROTOTYPE_v1.0.4_2013-11-25), NOAA Global Monitoring Division, Boulder, Colo., updated annually, doi:10.3334/OBSPACK/1001.

Olson, J. S., J. A. Watts, and L. J. Allison (1985), *Major World Ecosystem Complexes Ranked by Carbon in Live Vegetation (NDP-017)*, Carbon Dioxide Information Center, Oak Ridge Nat. Lab., Oak Ridge, Tenn.

Pan, Y., et al. (2011), A large and persistent carbon sink in the world's forests, *Science*, *333*(6045), 988–993, doi:10.1126/science.1201609.

Parazoo, N. C., et al. (2013), Interpreting seasonal changes in the carbon balance of southern Amazonia using measurements of XCO_2 and chlorophyll fluorescence from GOSAT, *Geophys. Res. Lett.*, *40*, 2829–2833, doi:10.1002/grl.50452.

Patil, D. J., B. R. Hunt, E. Kalnay, J. A. Yorke, and E. Ott (2001), Local low dimensionality of atmospheric dynamics, *Phys. Rev. Lett.*, *86*(26), 5878, doi:10.1103/PhysRevLett.86.5878.

Peters, W., M. C. Krol, E. J. Dlugokencky, F. J. Dentener, P. Bergamaschi, G. Dutton, P. van Velthoven, J. B. Miller, L. Bruhwiler, and P. P. Tans (2004), Toward regional-scale modeling using the two-way nested global model TM5: Characterization of transport using SF_6, *J. Geophys. Res.*, *109*, D19314, doi:10.1029/2004JD005020.

Peters, W., J. B. Miller, J. Whitaker, A. S. Denning, A. Hirsch, M. C. Krol, D. Zupanski, L. Bruhwiler, and P. P. Tans (2005), An ensemble data assimilation system to estimate CO_2 surface fluxes from atmospheric trace gas observations, *J. Geophys. Res.*, *110*, D24304, doi:10.1029/2005JD006157.

Peters, W., et al. (2007), An atmospheric perspective on North American carbon dioxide exchange: CarbonTracker, *Proc. Natl. Acad. Sci. U.S.A.*, *104*, 18,925–18,930, doi:10.1073/pnas.0708986104.

Peylin, P., P. Bousquet, C. Le Quéré, S. Sitch, P. Friedlingstein, G. McKinley, N. Gruber, P. Rayner, and P. Ciais (2005), Multiple constraints on regional CO_2 flux variations over land and oceans, *Global Biogeochem. Cycles*, *19*, GB1011, doi:10.1029/2003GB002214.

Phillips, O. L., and S. L. Lewis (2014), Evaluating the tropical forest carbon sink, *Global Change Biol.*, *20*(7), 2039–2041, doi:10.1111/gcb.12423.

Phillips, O. L., et al. (2009), Drought sensitivity of the amazon rainforest, *Science*, *323*(5919), 1344–1347, doi:10.1126/science.1164033.

Phillips, O. L., et al. (2010), Drought–mortality relationships for tropical forests, *New Phytol.*, *187*(3), 631–646, doi:10.1111/j.1469-8137.2010.03359.x.

Piao, S., et al. (2013), Evaluation of terrestrial carbon cycle models for their response to climate variability and to CO_2 trends, *Global Change Biol.*, *19*(7), 2117–2132, doi:10.1111/gcb.12187.

Potter, C., S. Klooster, C. Hiatt, V. Genovese, and J. C. Castilla-Rubio (2011), Changes in the carbon cycle of Amazon ecosystems during the 2010 drought, *Environ. Res. Lett.*, *6*(3), 034024, doi:10.1088/1748-9326/6/3/034024.

Potter, C. S., J. T. Randerson, C. B. Field, P. A. Matson, P. M. Vitousek, H. A. Mooney, and S. A. Klooster (1993), Terrestrial ecosystem production: A process model based on global satellite and surface data, *Global Biogeochem. Cycles*, *7*(4), 811–841, doi:10.1029/93GB02725.

Pyle, E. H., et al. (2008), Dynamics of carbon, biomass, and structure in two Amazonian forests, *J. Geophys. Res.*, *113*, G00B08, doi:10.1029/2007JG000592.

Richey, J. E., J. M. Melack, A. K. Aufdenkampe, V. M. Ballester, and L. L. Hess (2002), Outgassing from Amazonian rivers and wetlands as a large tropical source of atmospheric CO_2, *Nature*, *416*(6881), 617–620, doi:10.1038/416617a.

Saatchi, S., W. Buermann, H. ter Steege, S. Mori, and T. B. Smith (2008), Modeling distribution of Amazonian tree species and diversity using remote sensing measurements, *Remote Sens. Environ.*, *112*(5), 2000–2017, doi:10.1016/j.rse.2008.01.008.

Saatchi, S., S. Asefi-Najafabady, Y. Malhi, L. E. O. C. Aragão, L. O. Anderson, R. B. Myneni, and R. Nemani (2013), Persistent effects of a severe drought on Amazonian forest canopy, *Proc. Natl. Acad. Sci. U.S.A.*, *110*, 565–570, doi:10.1073/pnas.1204651110.

Saleska, S. R., et al. (2003), Carbon in Amazon Forests: Unexpected seasonal fluxes and disturbance-induced losses, *Science*, *302*(5650), 1554–1557, doi:10.1126/science.1091165.

Schaefer, K., G. J. Collatz, P. Tans, A. S. Denning, I. Baker, J. Berry, L. Prihodko, N. Suits, and A. Philpott (2008), Combined simple biosphere/Carnegie-Ames-Stanford approach terrestrial carbon cycle model, *J. Geophys. Res.*, *113*, G03034, doi:10.1029/2007JG000603.

Sellers, P. J., D. A. Randall, G. J. Collatz, J. A. Berry, C. B. Field, D. A. Dazlich, C. Zhang, G. D. Collelo, and L. Bounoua (1996), A revised land surface parameterization (SiB2) for atmospheric GCMs. Part I: Model formulation, *J. Clim.*, *9*(4), 676–705, doi:10.1175/1520-0442(1996)009<0676:ARLSPF>2.0.CO;2.

Stephens, B. B., et al. (2007), Weak northern and strong tropical land carbon uptake from vertical profiles of atmospheric CO_2, *Science*, *316*(5832), 1732–1735, doi:10.1126/science.1137004.

Tiedtke, M. (1989), A comprehensive mass flux scheme for cumulus parameterization in large-scale models, *Mon. Weather Rev.*, *117*(8), 1779–1800, doi:10.1175/1520-0493(1989)117<1779:ACMFSF>2.0.CO;2.

van der Velde, I. R. (2015), Studying biosphere-atmosphere exchange of CO_2 through Carbon-13 stable isotopes, PhD thesis, Wageningen University, Wageningen, Netherlands, 5 June.

van der Velde, I. R., J. B. Miller, K. Schaefer, G. R. van der Werf, M. C. Krol, and W. Peters (2014), Terrestrial cycling of $^{13}CO_2$ by photosynthesis, respiration, and biomass burning in SiBCASA, *Biogeosciences*, *11*, 6553–6571, doi:10.5194/bg-11-6553-2014.

van der Werf, G. R., J. T. Randerson, L. Giglio, N. Gobron, and A. J. Dolman (2008), Climate controls on the variability of fires in the tropics and subtropics, *Global Biogeochem. Cycles*, *22*, GB3028, doi:10.1029/2007GB003122.

van der Werf, G. R., J. T. Randerson, L. Giglio, G. J. Collatz, M. Mu, P. S. Kasibhatla, D. C. Morton, R. S. Defries, Y. Jin, and T. T. van Leeuwen (2010), Global fire emissions and the contribution of deforestation, savanna, forest, agricultural, and peat fires (1997–2009), *Atmos. Chem. Phys.*, *10*(23), 11,707–11,735, doi:10.5194/acp-10-11707-2010.

van Leeuwen, T. T., W. Peters, M. C. Krol, and G. R. van der Werf (2013), Dynamic biomass burning emission factors and their impact on atmospheric CO mixing ratios, *J. Geophys. Res. Atmos.*, *118*, 6797–6815, doi:10.1002/jgrd.50478.

Vilà-Guerau de Arellano, J., B. Gioli, F. Miglietta, H. J. J. Jonker, H. K. Baltink, R. W. A. Hutjes, and A. A. M. Holtslag (2004), Entrainment process of carbon dioxide in the atmospheric boundary layer, *J. Geophys. Res.*, *109*, D18110, doi:10.1029/2004JD004725.

Wang, W., P. Ciais, R. R. Nemani, J. G. Canadell, S. Piao, S. Sitch, M. A. White, H. Hashimoto, C. Milesi, and R. B. Myneni (2013), Variations in atmospheric CO_2 growth rates coupled with tropical temperature, *Proc. Natl. Acad. Sci. U.S.A.*, *110*, 15163, doi:10.1073/pnas.1219683110.

Whitaker, J. S., and T. M. Hamill (2002), Ensemble data assimilation without perturbed observations, *Mon. Weather Rev.*, *130*(7), 1913–1924, doi:10.1175/1520-0493(2002)130<1913:EDAWPO>2.0.CO;2.

Wiedinmyer, C., S. K. Akagi, R. J. Yokelson, L. K. Emmons, J. A. Al-Saadi, J. J. Orlando, and A. J. Soja (2011), The Fire INventory from NCAR (FINN): A high resolution global model to estimate the emissions from open burning, *Geosci. Model Dev.*, *4*, 625, doi:10.5194/gmd-4-625-2011.

Xu, L., A. Samanta, M. H. Costa, S. Ganguly, R. R. Nemani, and R. B. Myneni (2011), Widespread decline in greenness of Amazonian vegetation due to the 2010 drought, *Geophys. Res. Lett.*, *38*, L07402, doi:10.1029/2011GL046824.